A. Baz

J. Ro

Mechanical Engineering Department
The Catholic University of America
Washington, DC 20064

Performance Characteristics of Active Constrained Layer Damping

Theoretical and experimental performance characteristics of the new class of actively controlled constrained layer damping (ACLD) are presented. The ACLD consists of a viscoelastic damping layer sandwiched between two layers of piezoelectric sensor and actuator. The composite ACLD when bonded to a vibrating structure acts as a "smart" treatment whose shear deformation can be controlled and tuned to the structural response in order to enhance the energy dissipation mechanism and improve the vibration damping characteristics. Particular emphasis is placed on studying the performance of ACLD treatments that are provided with sensing layers of different spatial distributions. The effect of the modal weighting characteristics of these sensing layers on the broad band attenuation of the vibration of beams fully treated with the ACLD is presented theoretically and experimentally. The effect of varying the gains of a proportional and derivative controller and the operating temperature on the ACLD performance is determined for uniform and linearly varying sensors. Comparisons with the performance of conventional passive constrained layer damping are presented also. The results obtained emphasize the importance of modally shaping the sensor and demonstrate the excellent capabilities of the ACLD. © 1995 John Wiley & Sons, Inc.

INTRODUCTION

Passive constrained layer damping (PCLD) treatments have been successfully utilized as a simple and reliable means for damping out the vibration of a wide variety of flexible structures (Cremer et al., 1988). However, for effective performance over a broad range of temperatures and frequencies, the weight of PCLD treatments can pose serious limitation to their use in applications where weight is critical.

It is therefore the purpose of this article to consider the new class of active constrained layer damping (ACLD) treatment (Baz, 1992, 1993; Baz and Ro, 1993a,b, 1994) that has a high energy dissipation-to-weight ratio as compared to conventional constrained damping layers. The ACLD combines the attractive attributes of both the passive and active controls to achieve optimal vibration damping. In particular, it provides an effective means for augmenting the simplicity and reliability of passive damping with the low weight and high efficiency of active controls to attain high damping characteristics over broad frequency bands. Such characteristics are particularly suitable for damping the vibration of critical systems such as rotorcraft blades where damping-to-weight ratio is very important.

In the present study, the emphasis is placed on developing and experimentally validating a finite

element model (FEM) that describes the behavior of the ACLD treatment with sensing layers of spatially varying distributions. This is in contrast to the distributed-parameter models and FEMs developed in the previous studies for ACLD with uniform sensors (Baz, 1993; Baz and Ro, 1993a,b). The FEM enhances the practicality of predicting the behavior of structures subject to a wide variety of boundary conditions and partially treated with multi-patches of ACLD treatments. The model also allows the prediction of the ACLD performance when specific modes are targeted with proper spatial shaping of the sensing layer.

CONCEPT OF ACLD

The proposed ACLD (Fig. 1), consists of a conventional PCLD augmented with efficient active control means to control the strain of the constrained layer, in response to the structural vibrations. The viscoelastic damping layer is sandwiched between two piezoelectric layers. The three-layer composite ACLD when bonded to the beam acts as a "smart" constraining layer damping treatment with built-in sensing and actuation capabilities. The sensing, as indicated by the sensor voltage V_s, is provided by the piezoelectric layer directly bonded to the beam surface. The actuation is generated by the other piezoelectric layer that acts as an active constraining layer that is activated by the control voltage V_c. With appropriate strain control, through proper manipulation of V_s, the shear deformation of the viscoelastic damping layer can be increased, the energy dissipation mechanism can be enhanced, and the structural vibration can be damped.

In this manner, the ACLD provides a practical means for controlling the vibration of massive structures with currently available piezoelectric actuators without the need for excessively large actuation voltages. This is due to the fact that the

ACLD properly utilizes the piezoelectric actuator to control the shear in the soft viscoelastic core, a task compatible with the low control authority capabilities of the currently available piezoelectric materials.

THEORETICAL MODELING OF ACLD

Overview

An FEM was developed to describe the behavior of beams with ACLD treatments. The model extends the studies of Trompette et al. (1978) and Rao (1976) that have been used to analyze the dynamics of PCLD. It accounts for the behavior of the distributed and spatially shaped piezoelectric sensor (Miller and Hubbard, 1986) and the distributed piezoelectric actuator (Crawley and de Luis, 1987). Appropriate control laws are considered to control the interaction between the piezo-sensor and actuator in order to achieve enhanced vibration control characteristics.

The emphasis of the present study was placed on the development of a model for Bernoulli–Euler beams that were treated with multipatches of ACLD layer in order to demonstrate the feasibility and merits of the ACLD concept. ACLD treatments with uniform and spatially shaped sensors are considered in the following analyses in order to investigate the potential of targeting specific modes with the shaped sensors.

The Model

Figure 2(a) shows a schematic drawing of the ACLD treatment of a sandwiched beam divided into N finite elements. It is assumed that the shear strains in the piezoelectric sensor/actuator layers and in the base beam are negligible. The transverse displacements w of all points on any cross section of the sandwiched beam are considered to be equal. Furthermore, the piezoelectric sensor/actuator layers and the base beam are as-
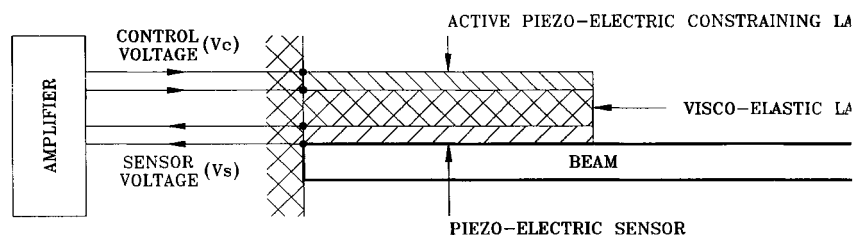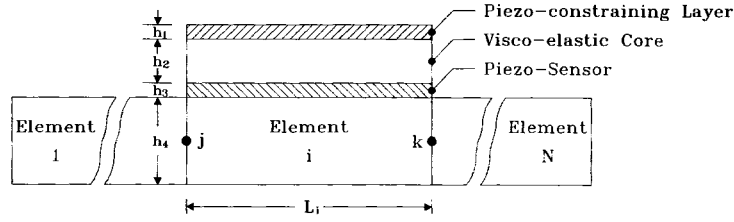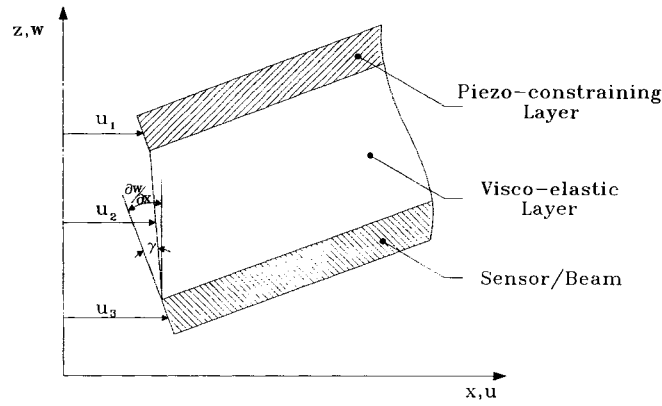

FIGURE 1 Schematic drawing of the active constrained layer damping.

FIGURE 2 Finite element model of a beam treated with the active constrained layer damping: (a) main configuration, (b) deflections.

sumed to be elastic and to dissipate no energy, whereas the core is assumed to be linearly viscoelastic. In addition, the piezoelectric sensor and the base beam are considered to be perfectly bonded together such that they can be reduced to a single equivalent layer. Accordingly, the original four-layer sandwiched beam reduces to an equivalent three-layer beam.

Basic Kinematic Relationships. From the geometry of Fig. 2(b), the shear strain γ of the viscoelastic core is given by:

$$\gamma = \frac{d}{h_2}\frac{\partial w}{\partial x} + \frac{(u_1 - u_3)}{h_2} \qquad (1)$$

where

$$d = h_2 + \frac{h_1}{2} + D \qquad (2)$$

with D denoting the distance from the neutral axis of the beam/sensor layer to the interface with the viscoelastic layer. Also, h_1 and h_2 denote the thicknesses of the piezo-actuator and the viscoelastic layer, respectively. Figure 2(b) indicates also that the longitudinal deflection u_2 of the viscoelastic core is given by:

$$u_2 = \frac{1}{2}\left[(u_1 + u_3) + (h_{1/2} - D)\frac{\partial w}{\partial x}\right]. \qquad (3)$$

Shape Functions. The spatial distributions of the longitudinal displacements u_1 and u_3 and the transverse deflection w over any element i of the treated beam, are assumed to be given by:

$$u_1 = a_1x + a_2, u_3 = a_3x + a_4 \quad \text{and}$$
$$w = a_5x^3 + a_6x^2 + a_7x + a_8 \qquad (4)$$

where the constants $\{a_1, a_2, \ldots, a_8\} = \{a\}$ are determined in terms of the eight components of the nodal deflection vector $\{\Delta_i\}$ of the ith element bounded between nodes j and k. The nodal deflection vector $\{\Delta_i\}$ is given by

$$\{\Delta_i\} = \{u_{1j}, u_{3j}, w_j, w_j', u_{1k}, u_{3k}, w_k, w_k'\}^T \quad (5)$$

with the primes denoting spatial derivatives. Therefore, the deflection $\{\Delta\} = \{u_1, u_3, w, w'\}^T$ at any location x along the ith element can be determined from:

$$\{u_1, u_3, w, w'\}^T = \{N_1, N_2, N_3, N_4\}^T\{\Delta_i\} \quad (6)$$

where N_1, N_2, N_3, and N_4 are the spatial interpolating vectors corresponding to u_1, u_3, w, and w', respectively.

Strain Energies. The strain energies associated with the various layers of the ACLD treatment are determined as follows.

Constraining layer: The energies include:

extension

$$U_1 = \frac{1}{2} E_1 A_1 \{\Delta_i\}^T \left[\int_{L_i} [N_1']^T[N_1'] \, dx \right] \{\Delta_i\} \quad (7)$$

where E_1 and A_1 are the modulus of elasticity and area of cross section of the constraining layer.

bending

$$U_2 = \frac{1}{2} E_1 I_1 \{\Delta_i\}^T \left[\int_{L_i} [N_3'']^T[N_3''] \, dx \right] \{\Delta_i\} \quad (8)$$

where $E_1 I_1$ is the flexural rigidity of the constriaining layer.

Viscoelastic layer: The energies include

extension

$$U_3 = \frac{1}{2} E_2 A_2 \{\Delta_i\}^T \left[\int_{L_i} [N_5]^T[N_5] \, dx \right] \{\Delta_i\} \quad (9)$$

where E_2 and A_2 are the modulus of elasticity and area of cross section of the viscoelastic layer. Also $[N_5]$ is an interpolating matrix $= ([N_1'] + [N_2'] + (h_1/2 - D)[N_3''])/2$.

bending

$$U_4 = \frac{1}{2} E_2 I_2 \{\Delta_i\}^T \left[\int_{L_i} [N_6]^T[N_6] \, dx \right] \{\Delta_i\} \quad (10)$$

where $E_2 I_2$ is the flexural rigidity of the viscoelastic layer and an interpolating matrix $[N_6] = ([N_1'] - [N_2'] + (h_1/2 + D)[N_3''])/h_2$.

shearing

$$U_5 = \frac{1}{2} G_2 A_2 \{\Delta_i\}^T \left[\int_{L_i} [N_7]^T[N_7] \, dx \right] \{\Delta_i\} \quad (11)$$

where G_2 is the shear modulus of the viscoelastic layer. Also an interpolating matrix $[N_7] = ([N_1'] - [N_2'] + d[N_3''])/h_2$.

Sensor/beam layer: The energies include

extension

$$U_6 = \frac{1}{2} E_e A_e \{\Delta_i\}^T \left[\int_{L_i} [N_2']^T[N_2'] \, dx \right] \{\Delta_i\} \quad (12)$$

where E_e and A_e are the modulus of elasticity and area of cross section of the sensor/beam layer.

$$U_7 = \frac{1}{2} E_e I_e \{\Delta_i\}^T \left[\int_{L_i} [N_3'']^T[N_3''] \, dx \right] \{\Delta_i\} \quad (13)$$

where $E_e I_e$ is the flexural rigidity of the sensor/ beam layer.

From Eqs. (7)–(13), the total strain energy U can be written as:

$$U = \sum_{i=1}^{7} U_i = \frac{1}{2} \{\Delta_i\}^T [K_i]\{\Delta_i\} \quad (14)$$

where $[K_i]$ is the equivalent stiffness matrix of the ith element.

Kinetic Energies. **Constraining layer:** It is given by:

$$T_1 = \frac{1}{2} \rho_1 A_1 \int_{L_i} (\dot{w}^2 + \dot{u}_1^2) \, dx = \frac{1}{2} \rho_1 A_1 \{\dot{\Delta}_i\}^T$$
$$\left[\int_{L_i} ([N_3]^T[N_3] + [N_1]^T[N_1]) \, dx \right] \{\dot{\Delta}_i\} \quad (15)$$

where ρ_1 is the density of the constraining layer.
Viscoelastic layer: It is given by:

$$T_2 = \frac{1}{2} \rho_2 A_2 \int_{L_i} (\dot{w}^2 + \dot{u}_2^2) \, dx = \frac{1}{2} \rho_2 A_2 \{\dot{\Delta}_i\}^T$$
$$\left[\int_{L_i} ([N_3]^T[N_3] + [N_8]^T[N_8]) \, dx \right] \{\dot{\Delta}_i\} \quad (16)$$

where ρ_2 is the density of the viscoelastic layer and $[N_8] = ([N_1] + [N_2] + (h_1/2 - D)[N_3'])/2$.

Sensor/beam layer: It is given by:

$$T_3 = \frac{1}{2} \rho_e A_e \int_{L_i} (\dot{w}^2 + \dot{u}_3^2)\, dx = \frac{1}{2} \rho_e A_e \{\dot{\Delta}_i\}^T$$

$$\left[\int_{L_i} ([N_3]^T[N_3] + [N_2]^T[N_2])\, dx \right] \{\dot{\Delta}_i\} \quad (17)$$

where ρ_e is the density of the sensor/beam layer.

From Eqs. (15)–(17), the total kinetic energy T can be written as:

$$T = \sum_{i=1}^{3} T_i = \frac{1}{2} \{\dot{\Delta}_i\}^T [M_i]\{\dot{\Delta}_i\} \quad (18)$$

where $[M_i]$ is the equivalent mass matrix of the ith element.

Piezo-Control Forces and Moments. Piezo-actuator:
The strain ε_p induced in the piezoelectric actuator is given by (Crawley and de Luis, 1987):

$$\varepsilon_p = \left(\frac{d_{31}}{h_1} \right) V_c \quad (19)$$

where d_{31} is the piezoelectric strain constant resulting from the application of the voltage V_c across the piezo-actuator layer. In Eq. (19), V_c is assumed constant over the length of the beam element. The voltage V_c is generated from the proper manipulation of the piezo-sensor voltage V_s.

Piezo-sensor: The strain ε_s induced in the piezo-sensor is proportional to the beam curvature (d^2w/dx^2) and is given by:

$$\varepsilon_s = -D_d \frac{\partial^2 w}{\partial x^2} \quad (20)$$

where D_d is the distance from the beam neutral axis to the sensor surface.

The induced strain ε_p integrated over the entire length of the sensor due to its distributed nature, generates an output voltage V_s given by Miller and Hubbard (1987):

$$V_s = -\left[\frac{k_{31}^2 D_d b}{g_{31} C} \right] \sum_{i=i_s}^{i_f} \int_0^{L_i} f_i(x) \frac{\partial^2 w}{\partial x^2}\, dx \quad (21)$$

where $f_i(x)$ is a spatial distribution function that defines the shaping of the sensor over element i. For uniform sensor $f_i(x) = 1$ and for a linearly shaped sensor $f_i(x) = 1 - x/L$ as shown in Fig.

(3). In Eq. (21), the sensor is extended between elements i_s and i_f. Also, k_{31} is the electromechanical coupling factor, g_{31} is the piezoelectric voltage constant, and C is the capacitance of the sensor given by:

$$C = 8.854(10^{-12}) A \frac{K_{3t}}{h_3} \quad (22)$$

where A is the sensor surface area and k_{3t} is the dimensionless dielectric constant.

Control law: The manipulation of the piezo-sensor voltage V_s to generate the actuator voltage V_c is governed by the following proportional and derivative control law:

$$V_c = -\left(K_p V_s + K_d \frac{dV_s}{dt} \right) G_e(\omega) \quad (23)$$

where K_p and K_d are the proportional and derivative control gains, respectively. Also $G_e(\omega)$ denotes the transfer function of the power amplifier.
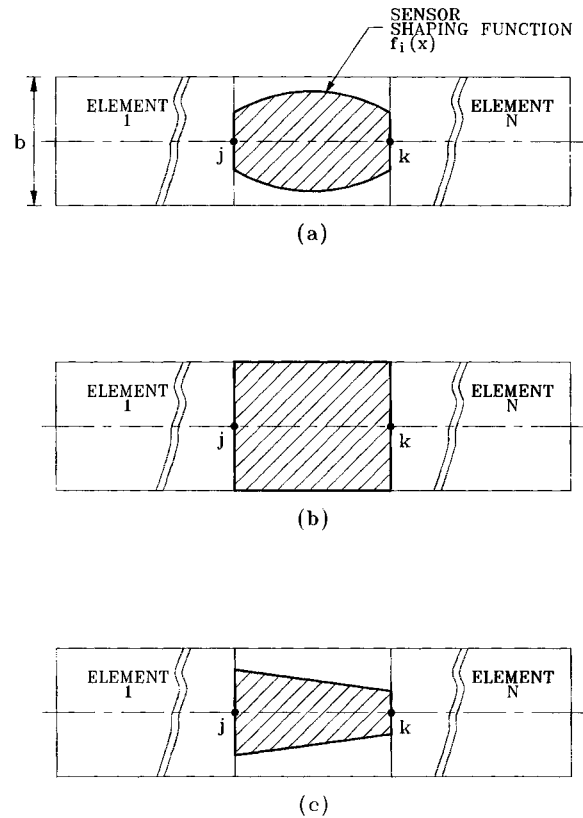

(a)

(b)

(c)

FIGURE 3 Schematic drawing of sensor configurations: (a) generally shaped, (b) uniform, (c) linearly shaped.

Control forces and moments: The vector $\{F_c\}$ of the control forces and moments generated by the piezo-constraining layer on the treated beam element can be expressed in the following matrix form:

$$\{F_c\} = \{F_{pj}, 0, F_{wj}, M_{pj}, F_{pk}, 0, F_{wk}, M_{pk}\}^T \quad (24)$$

where F_{pj}, F_{pk}, M_{pj}, and M_{pk} denote the control forces and moments generated at nodes j and k given *for the uniform sensor*:

$$F_{pj} = -F_{pk} = \frac{-g}{2}(K_P + K_dp)(w'_{i_s} - w'_{i_r+1})$$

$$F_{wj} = F_{wk} = 0 \quad \text{and}$$

$$M_{pj} = -M_{pk} = -g(K_P + K_dp) \quad (25)$$

$$\left[\frac{1}{2}(u_{1i_s} - u_{1i_r+1}) - D_1(w'_{i_s} - w'_{i_r+1})\right]$$

for the shaped sensor:

$$F_{pj} = -F_{pk} = \frac{-g}{2L_s}(K_P + K_dp)[(w_{i_s}$$

$$- w_{i_r+1}) + L_s w'_{i_s}]$$

$$F_{wj} = F_{wk} = \frac{-g}{2L_s}(K_P + K_dp)[(u_{1i_s}$$

$$- u_{1i_r+1}) - D_1(w'_{i_s} - w'_{i_r+1})]$$

$$M_{pj} = \frac{-g}{2}(K_P + K_dp)\left[(u_{1i_s} - u_{1i_r+1})\right] \quad (26)$$

$$- D_1(2w'_{i_s} - w'_{i_r+1}) - \frac{D_1}{L_s}(w_{i_s} - w_{i_r+1})\right] \quad \text{and}$$

$$M_{pk} = \frac{-D_1 g}{2}(K_P + K_dp)$$

$$\left[w'_{i_s} + \frac{1}{L_s}(w_{i_s} - w_{i_r+1})\right]$$

where $g = E_1 b^2 d_{31}[k_{31}^2 D_d/g_{31} C]G_e(\omega)$, D_1 is distance between neutral axis of entire sandwiched beam and piezo-actuator, and p is the d/dt operator. Also, L_s denotes sensor length.

Equations of Motion. The stiffness matrix $[K_i]$, the mass matrix $[M_i]$, and the control force vector $\{F_c\}$ are combined to describe the dynamics of the ACLD-treated beam element as follows:

$$[M_i]\{\ddot{\Delta}_i\} + [K_i]\{\Delta_i\} = \{F_c\}. \quad (27)$$

The effect of the proportional and derivative control actions on the performance of the assembled closed-loop system, given by Eq. (27), is determined by computing the eigenvalues (i.e., natural frequencies and damping ratios) of the closed-loop system and comparing these eigenvalues with those of the open-loop system. Experimental validation of the theoretical predictions is determined in the following section.

PERFORMANCE OF BEAMS WITH ACLD AND PCLD TREATMENTS

Experimental Setup

Figure 4 shows a schematic drawing of the experimental setup used in testing the effectiveness of the ACLD in attenuating the vibration of the test beam as compared to conventional PCLD. The setup is used also to investigate the performance of ACLD treatments with uniform and shaped sensors. The, beam under consideration is mounted in a cantilevered manner on an oscillating table excited by a shaker driven by a sinusoidal or white noise source through a power amplifier. The amplitude of vibration of the free end of the beam is monitored by a laser sensor (Model MQ, Aromat Crop., Providence, NJ) mounted on the oscillating table. The output signal of the laser sensor is sent to a spectrum analyzer to determine the vibration attenuation both in the time and frequency domains. The laser sensor has a precision of 20 μm over a frequency band between 0–1000 Hz. The test beam is 28.4 cm long, 3.08 cm wide, and 0.124 cm thick. It is made of a polymer that has density of 1.24 g cm^{-3} and Young's modulus of 4.25 GN/m^2. The first and second modes of vibration of the beam are 3.99 and 24.87 Hz. The corresponding modal damping ratios are 0.03 and 0.03, respectively. The beam is fully treated with an ACLD that consists of a viscoelastic sheet of DYAD-606 (SOUNDCOAT) sandwiched between two piezoelectric layers (AMP, Inc., Valley Forge, PA). Two sensors configurations were considered in this study. The first sensor is of uniform width [Fig. 3(a)] whereas the second sensor has a linearly varying width [Fig. 3(b)]. The length and thickness of the viscoelastic layer were 28.0 and 0.0508 cm, respectively. Its density is 1.104 g cm^{-3} and its complex shear modulus is both temperature and frequency dependent as indicated in SOUNDCOAT's bulletin number 810. All piezo-
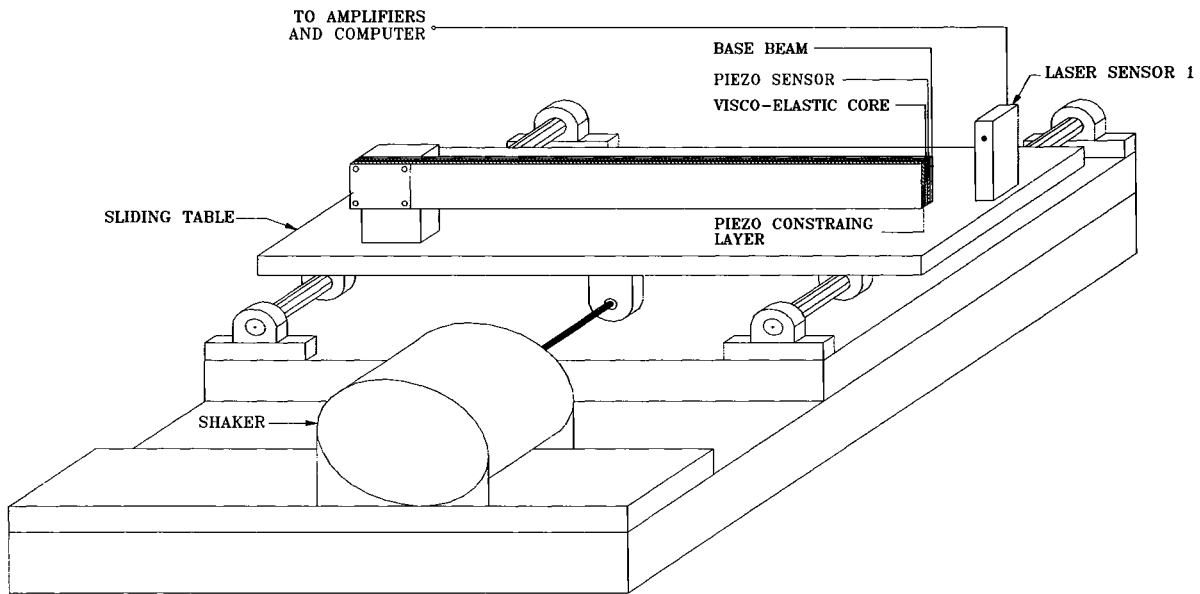
FIGURE 4 Schematic drawing of the experimental setup.

electric layers utilized are made from PVDF polymeric films (number S028NA). The length and thickness of the sensor and actuator layers were 28.0 and 0.0028 cm, respectively. The piezoelectric films have density $= 1.8 \, g \, cm^{-3}$, $d_{31} = 23 \times 10^{-12} \, m/V$, $k_{31} = 0.15$, $g_{31} = 216 \times 10^{-3} \, Vm/N$, $k_{3t} = 12$, and $E_{1,3} = 2.25 \, GN/m^2$ (AMP, Inc., Catalog No. 65751).

The signal from the piezoelectric sensor was sampled by a microprocessor via a charge amplifier (Model AM-5, Wilcoxon Research, Rockville, MD) and an input/output board (Model DASH-16, METRABYTE, Taunton, MA). The signal was manipulated inside the microprocessor using the proportional and derivative control law. The resulting control action was sent via the output board and an analog power amplifier (Model PA7C, Wilcoxon) to the piezoelectric constraining layer.

Experimental Results

Effect of Controller Gains. Figures 5 and 6 show the effect of varying the controller gains (K_P and K_d) on the amplitude of vibration of the free end of the tested beam when it is provided with a uniform or shaped sensor, respectively. The displayed results were obtained when the beam was subjected to broad-band random excitation. The figures also show the vibration amplitude of the beam when it was passively treated with the sandwiched viscoelastic damping treatment. In
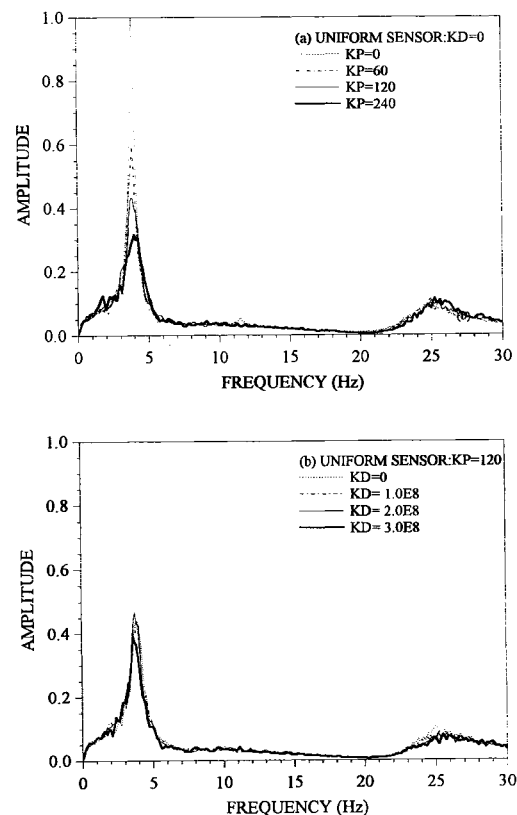

FIGURE 5 Effect of controller gains with uniform sensor.
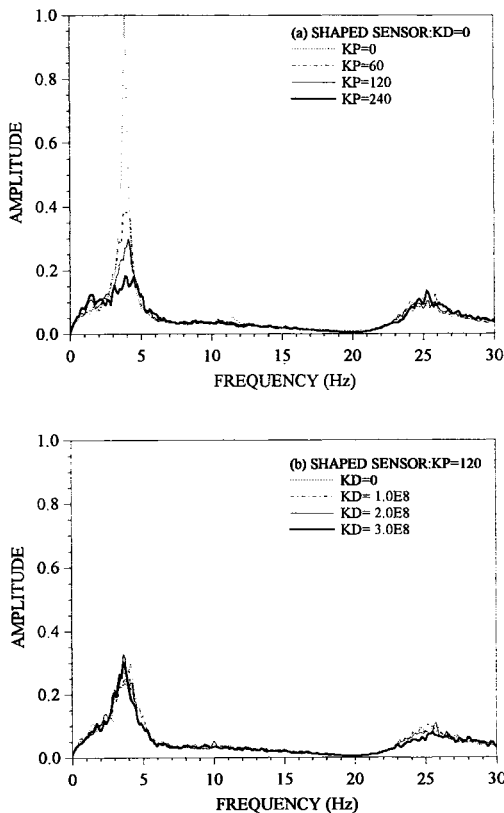
FIGURE 6 Effect of controller gains with shaped sensor.

that case, the control loop that regulates the interaction between the piezo-sensor and the piezo-actuator was maintained open (i.e., $K_P = 0$ and $K_d = 0$). It is evident from Fig. 5(a) that increasing the proportional controller gain K_P, for an ACLD with a uniform sensor, results in significant attenuation of the amplitude of vibration of the first mode. Further attenuation was observed when the proportional controller was augmented with a derivative component as shown in Fig. 5(b). However, the attenuation improved considerably by using the shaped sensor [Fig. 6(a)], particularly at the first mode of vibration. Such a result was expected as the linearly shaped sensor was found to be effective in targeting the first (odd) mode as reported in details by Miller and Hubbard (1987). The effectiveness of the shaped sensor is attributed to the fact that its output voltage and control actions are proportional to the tip deflection, as indicated by Eq. (26), rather than tip angular deflection as in the case of the uniform sensor governed by Eq. (25). This characteristic coupled with the fact that odd modes of cantilevered beams are characterized

by large deflections and small angular deflections makes the shaped sensor effectively target the odd modes. As for the uniform sensor, it becomes more effective in the case of the second (even) mode as the even modes are characterized, for a cantilevered beam, by large angular deflections and small transverse deflections.

Effect of Operating Temperature. The effect of varying the operating temperature on the performance of the ACLD with uniform and shaped sensors is shown in Fig. 7 when $K_P = 240$ and $K_d = 2E8$. The displayed results are obtained by subjecting the beam to a continuous sinusoidal sweep from 1 to 50 Hz. The figure emphasizes the effectiveness of the shaped sensor in targeting and suppressing the vibration of the first mode while the uniform sensor is more effective in attenuating the second mode. Furthermore, the figure indicates also that the ACLD is effec-
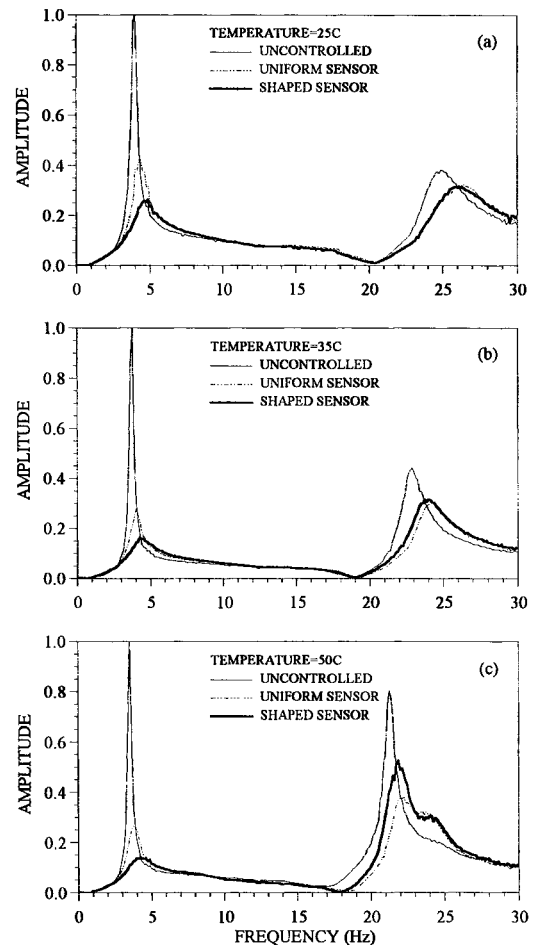

FIGURE 7 Effect of operating temperature on the ACLD performance.

tive in attenuating the vibration over a relatively wide temperature range.

Figure 8 summarizes comparisons between the experimental results and the theoretical predictions for the natural frequencies and damping ratios of the ACLD treatment with uniform and shaped sensors. The figure shows these comparisons for the first and second modes at three operating temperatures. It emphasizes the excellent agreement between the theoretical and experimental predictions. The theoretical results are obtained by dividing the beam into 10 finite elements and solving the resulting eigenvalue prob-
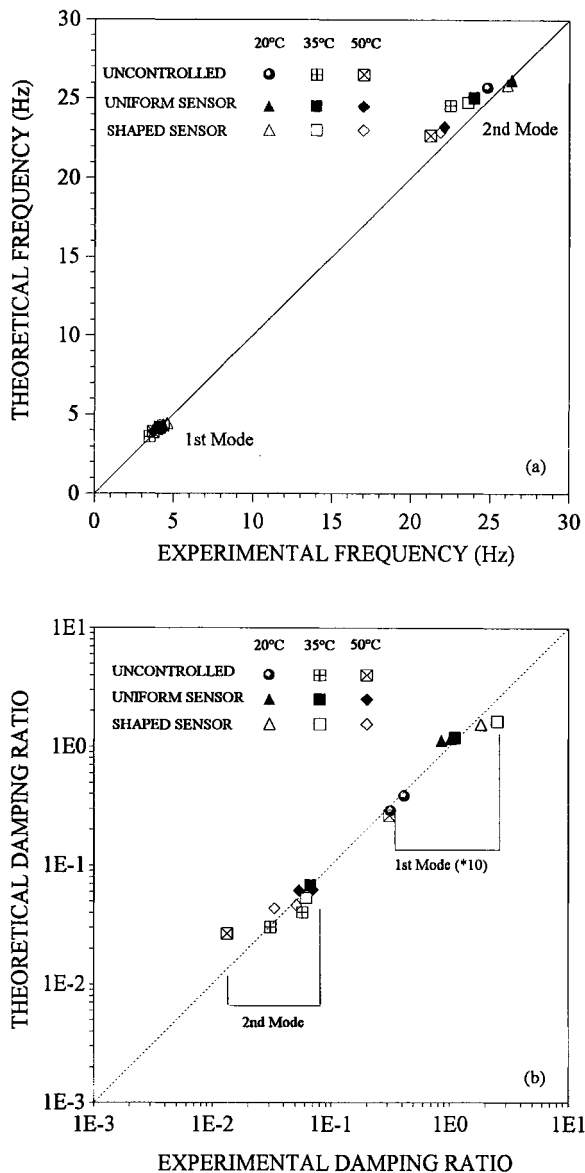
lem using the QR algorithm (IMSL Math. Library, 1994).
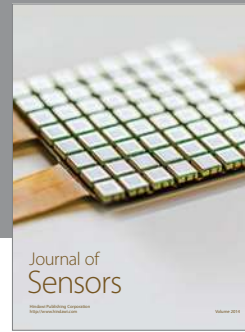
CONCLUSIONS

This article has presented a new class of ACLD treatment that consists of a conventional viscoelastic core augmented with built-in sensing and actuation capabilities. The equations governing the performance of this class of surface treatment, with uniform and spatially varying sensors, are presented using a finite element formulation. The theoretical predictions of the model are compared with the experimental performance of a computer-controlled beam treated with a DYAD 606 viscoelastic layer sandwiched between two layers of PVDF piezoelectric films. It is observed that ACLD with a linearly varying sensor is capable of targeting and suppressing the vibration of the first (odd) mode whereas ACLD with a uniform sensor is more effective for the second (even) mode. The effect of varying the gains of a proportional and derivative controller and the operating temperature on the ACLD performance is determined for both the uniform and linearly varying sensors. In the present study, the gains are maintained low to avoid control instabilities and spillover effects. Such effects are currently under investigation. Comparisons with the performance of conventional PCLD are presented and emphasize the favorable merits of the ACLD.

REFERENCES

Baz, A., 1993, "Active Constrained Layer Damping," U.S. Pat. application no. 08/136210.

Baz, A., 1993, "Active Constrained Layer Damping," *Proceedings of the DAMPING'93 Conference*, San Francisco, CA, Wright Laboratory Document no. WL-TR-93-3105, pp. IBB 1–23.

Baz, A., and Ro, J., 1993a, "Partial Treatment of Flexible Beams with Active Constrained Layer Damping," *Proceedings of the American Society of Mechanical Engineers*, No. AMD, Vol. 167, pp. 61–80.

Baz, A., and Ro, J., 1993b, "Finite Element Modeling and Performance of Active Constrained Layer

FIGURE 8 Comparisons between theoretical and experimental frequencies and damping ratios.

Damping," in L. Meirovitch, *Proceedings of the Ninth VPI & SU Conference on Dynamics & Control of Large Structures*, Blacksburg, VA, pp. 345–358.

Baz, A., and Ro, J., 1994, "Actively-Controlled Constrained Layer Damping," *Sound and Vibration Magazine*, Vol. 26, No. 3, pp. 18–21.

Crawley, E., and De Luis, J., 1987, "Use of Piezoelectric Actuators as Elements in Intelligent Structures," *Journal of AIAA*, Vol. 25, pp. 1373–1385.

Cremer, L., Heckel, M., and Ungar, E., 1988, *Structure-Borne Sound: Structural Vibrations and Sound Radiation at Audio Frequencies*, 2nd ed., Springer–Verlag, Berlin.

Miller, S., and Hubbard, J. Jr., 1987, "Observability of a Bernoulli–Euler Beam using PVF2 as a Distributed Sensor," in L. Meirovitch, *Proceedings of the Seventh Conference on Dynamics & Control of Large Structures*, VPI & SU, Blacksburg, VA, pp. 375–390.

Rao, D. K., 1976, "Static Response of Stiff-Cored Unsymmetric Sandwich Beams," *ASME Journal of Engineering for Industry*, Vol. 98, pp. 391–396.

Trompette, P., Boillot, D., and Ravanel, M.A., 1978, "The Effect of Boundary Conditions on the Vibration of a Viscoelastically Damped Cantilever Beam," *Journal of Sound and Vibration*, Vol. 60, No. 3, pp. 345–350.